Journal of Catalysis **200,** 298–308 (2001)
doi:10.1006/jcat.2001.3209, available online at http://www.idealibrary.com on IDEAL®

Effect of Drying Conditions of Au–Mn Co-Precipitates for Low-Temperature CO Oxidation

Seung-Jae Lee,* Asterios Gavriilidis,*,[1] Quentin A. Pankhurst,† Andreas Kyek,‡ Friederich E. Wagner,‡ Philip C. L. Wong,§ and King Lun Yeung¶

*Department of Chemical Engineering, University College London, Torrington Place, London WC1E 7JE, United Kingdom; †Department of Physics and Astronomy, University College London, Gower Street, London WC1E 6BT, United Kingdom; ‡Physik Department, Technische Universität München, D-85747 Garching, Germany; and §Material Characterization and Preparation Facility, and ¶Department of Chemical Engineering, The Hong Kong University of Science and Technology, Clear Water Bay, Kowloon, Hong Kong, People's Republic of China

Received October 13, 2000; revised February 8, 2001; accepted February 8, 2001; published online May 15, 2001

Au–Mn co-precipitates were dried at different temperatures and in different atmospheres. The co-precipitates were tested for low-temperature CO oxidation without any additional thermal treatment. While samples dried at 120°C in air exhibited the highest activity for CO oxidation, samples dried at room temperature under vacuum were less active. The catalytic properties of most fresh samples improved after the first light-off test, during which a temperature of 400°C was reached. To investigate the physical and chemical state of gold and manganese support, dried samples were examined by ^{197}Au Mössbauer spectroscopy, X-ray diffraction (XRD), transmission electron microscopy (TEM), and X-ray photoelectron spectroscopy (XPS). The ^{197}Au Mössbauer spectra showed that gold existed only in metallic form and was produced during the co-precipitation procedure. XRD and XPS analyses demonstrated that fresh samples contained manganese carbonate and oxides such as MnO_2. The carbonate was converted to manganese oxides after the light-off test. TEM analysis indicated that the manganese support was present in plate-like shapes and the shape of gold particles was rectangular with rounded corners. Au particle sizes were in the range 4.5–6.5 nm before the light-off test. After heat treatment at 400°C, catalytic activity improved and a strong interaction between gold particles and the MnO_x support was induced.

Key Words: **gold catalyst; carbon monoxide oxidation; co-precipitation; drying; manganese carbonate.**

INTRODUCTION

Gold supported on reducible oxides is known to catalyse CO oxidation at low temperatures (cf. 1, 2). This reaction could be important for CO safety gas masks (2), purification of air in CO_2 lasers (3), and CO sensors (4, 5). For example, Gardner's group reported that Au/MnO_x catalysts show better catalytic performance than Pt/SnO_2 (6–8). Torres Sanchez *et al.* (9) observed 100% CO conversion on Au/MnO_x catalysts in H_2 stream, which can be applicable for selective CO oxidation in H_2 streams of polymer electrolyte fuel cells.

Various preparation methods have been utilised to obtain active supported gold catalysts. Bamwenda *et al.* (10) reported that Au/TiO_2 prepared by conventional impregnation is considerably less active than Pt/TiO_2 prepared in the same way, but Au/TiO_2 prepared by deposition–precipitation exhibits better catalytic performance than platinum catalysts. Hutchings *et al.* (11) conducted durability tests of Au/ZnO prepared by co-precipitation and found that CO conversion was greater than 90% over 10 h of reaction time. Haruta's group prepared highly active supported gold catalysts by co-precipitation (12–15), deposition–precipitation (16–19), and chemical vapour deposition (20, 21). These preparation methods can produce small Au particles below 10 nm in size, which are strongly attached to metal oxide supports. Iwasawa's group (22–25) attempted to prepare supported gold catalysts using a gold–phosphine complex. Baiker's group (26–28) has prepared Au/TiO_2 and Au/ZrO_2 catalysts using gold sol formed by reduction of $HAuCl_4$ with tetrakis(hydroxymethyl)phosphonium chloride.

Co-precipitation of supported gold catalysts is usually performed by adding an aqueous solution of $HAuCl_4$ and a metal nitrate into an aqueous solution of Na_2CO_3. The co-precipitates formed are washed, dried, and calcined in air at a temperature above 250°C. However, it has been found that the preparation conditions such as precursor concentrations, pH, calcination temperature, and atmosphere can significantly influence catalyst activity for CO oxidation (7, 12, 29, 30).

For Au/MnO_x catalysts, Hoflund *et al.* (7) suggested that the ratio of Au to Mn in the precursor solution must be properly chosen to obtain high CO conversion. In their study, they reported that the optimum Au to Mn molar ratio in the precursor solution is 1 : 10. This observation is

[1] To whom correspondence should be addressed. E-mail: a.gavriilidis@ucl.ac.uk. Fax: +44-20-7383-2348.

0021-9517/01 $35.00

consistent with Haruta's assertion that the total surface area of exposed Au metal increases initially with Au content, but may decline when the gold loading increases further due to the coagulation of Au particles (13).

With regard to the effect of pH, Wagner *et al.* (29) reported that the sequence of mixing of precursor and alkaline solutions can affect the performance of the final catalyst. In their work, adding the precursor solution of gold and iron with low pH to an alkaline solution led to high activity of co-precipitates, while the so-called "inverse co-precipitation", i.e., adding the alkaline solution into the precursor solution, resulted in a less active catalyst. Catalyst activity was found to increase with the relative amount of ferrihydrite present.

Haruta *et al.* (12, 14) found that Au/Fe_2O_3 catalyst exhibited higher activity for CO oxidation after calcination at 300°C than at other temperatures in the range 80–500°C. Sintering of Au particles above 300°C and existence of a less active oxidic gold form below this temperature may have given rise to the observed maximum. Cunningham *et al.* (30) demonstrated with regard to calcination atmosphere that Au/TiO_2 catalysts calcined in air had higher activity, as compared to those calcined in vacuum.

Tanielyan and Augustine (31) prepared gold co-precipitates and subjected them to various heat and oxygen treatments. They observed that the most active catalysts were those dried at 95°C and then heated in oxygen at 200°C. Studies of Au/MnO_x catalysts showed that CO conversion is enhanced by pretreatment, leading to high hydroxyl group concentration on the catalyst surface, which may play an active role during the reaction (6, 32, 33).

All the above studies illustrate that there are various preparation parameters that can affect the activity of Au-supported catalysts. In this work, we address the effect of drying conditions such as drying atmosphere and temperature for Au/MnO_x, which is one of the most active gold catalyst systems (3). Catalyst performance for CO oxidation is investigated before and after high-temperature treatment.

EXPERIMENTAL

Catalyst Preparation

The gold catalysts were prepared by co-precipitation similar to the procedure used by Torres Sanchez *et al.* (9). A 20-ml solution of 0.01 M chloroauric acid ($HAuCl_4 \cdot xH_2O$, Alfa) and 40 ml of 0.1 M manganese nitrate [$Mn(NO_3)_2 \cdot 4H_2O$, Alfa] solution were mixed. The resulting solution was added dropwise to 60 ml of 0.1 M sodium carbonate (Na_2CO_3, Alfa) solution at room temperature with vigorous stirring. The fine suspension formed was aged for 15 min at room temperature. The final pH of the aged solution before filtration was about 9. The precipitate was filtered and washed with 500 ml of hot distilled water to remove the chloride ions that might affect catalytic activity. To investigate the effect of drying, the washed precipitates were divided into four parts and were dried for 15 h in static air at 120°C (H-A-120), in static air at 30°C (H-A-30), in vacuum at 30°C (H-V-30), and in hydrogen at 30°C (H-H-30) as summarised in Table 1. The bulk atomic ratio of Au to Mn was found to be 0.12 by X-ray fluorescence analysis (Jordan Valley EX-3600).

TABLE 1

Preparation Conditions of Au/MnO_x Catalysts and Corresponding CO Conversion at 25°C

Sample	Drying atmosphere	Drying temperature (°C)	CO conversion (%) at 25°C	
			1st run	2nd run
H-A-120	Static air	120	76	96
H-A-30	Static air	30	44	72
H-V-30	Vacuum	30	8	56
H-H-30	Hydrogen	30	10	20

CO Oxidation

The catalyst activity was measured in a continuous flow reactor at atmospheric pressure. The reactor was an 8-mm-i.d. quartz tube. Two thermocouples were placed before and after the catalyst powder to monitor the temperature of the inlet and outlet gas stream. As the difference between these temperatures was less than 1°C during reaction, the reactor can be considered to operate isothermally. The catalyst weight was fixed at 0.15 g, and the space velocity was maintained constant at 20,000 h^{-1}. The catalytic activities of the samples were compared by measuring CO conversion as a function of temperature (light-off test). This was performed with a mixture of 1% CO and 0.5% O_2 balanced by N_2 at a total flow rate of 50 ml/min. The CO passed through a column packed with γ-alumina pellets to remove metal carbonyls. The CO concentration of the reactor outlet was analysed on-line by a N.D.I.R. CO analyser (AAL model 401). During the light-off test, the signal from the CO analyser and the temperature of the catalyst bed were monitored using a personal computer. The light-off test was performed on the sample immediately after drying (*1st run*). During the light-off test the temperature of the furnace was raised from room temperature to 400°C at a heating rate of 5°C/min and was held at 400°C for 30 min. After the catalyst bed was cooled to room temperature, the procedure was repeated (*2nd run*). A change in activity was expected in the 2nd run because the catalyst had been exposed to high temperature during the 1st run.

Catalyst Characterisation

X-ray diffraction (XRD). To obtain information about catalyst composition, XRD was carried out using synchrotron radiation (wavelength = 0.6920 Å) as the X-ray source on Station 9.1 at the CLRC Daresbury Laboratory, U.K. Samples were contained in 0.5-mm capillary glass tubes and exposed to the radiation for 20 min to take an X-ray diffraction image using a high-resolution curved image plate. The developed image was converted to an X-ray diffraction pattern using Si as the calibration standard. The gold particle size was calculated based on Scherrer's equation.

Transmission electron microscopy (TEM). The size and morphology of the catalyst were characterised using a Philips CM20 transmission electron microscope. For the TEM imaging, the catalyst powder was dispersed in acetone and a drop of the suspension was placed onto the carbon-coated grid. The excess liquid was removed using a paper wick and the deposit was dried in air prior to imaging. Elemental composition of the sample was determined *in situ* using a Philips L200C energy-dispersive X-ray spectrometer (EDXS). The mean diameter of Au particles was determined by measuring the size of 50–120 particles in the TEM micrographs.

^{197}Au Mössbauer spectroscopy. The chemical state of gold in selected samples was determined by ^{197}Au Mössbauer spectroscopy. The ^{197}Pt isotope ($T_{1/2} = 18$ h) feeding the 77-keV Mössbauer transition of ^{197}Au was prepared by neutron activation of isotopically enriched ^{196}Pt metal. The Mössbauer measurements were performed in a liquid helium bath cryostat with both the source and the absorber at 4.2 K. All isomer shifts were calibrated with respect to the Pt metal source. The spectra of all samples were fitted with a single Lorentzian line. To determine the chemical state of Au *before drying*, measurements were performed with a sample quenched in liquid nitrogen immediately after co-precipitation.

X-ray photoelectron spectroscopy (XPS). The surface composition of the catalysts was analysed using X-ray photoelectron spectroscopy (Physical Electronics Model PHI 5600). The XPS spectra were acquired using monochromatic Al $K\alpha$ X-ray source operated at 350 W. Survey spectra were collected over the range 0–1400 eV with a pass energy of 187.85 eV. High-resolution XPS spectra were acquired for C 1*s*, O 1*s*, Mn 2*p*, and Au 4*f* using pass energy equal to 23.50 eV. In all cases, the photoelectron take-off angle was 45°. The XPS spectra were corrected internally using C 1*s* (285.0 eV) as the sample charging can shift the peak locations in the XPS spectra. The relative composition of each specimen was calculated from the relative XPS peak areas. A Au $4f_{7/2}$ binding energy of 84.1 eV was obtained from Au (150 nm) coated silicon and was used as the standard reference for metallic Au.

RESULTS

CO Oxidation

Light-off tests were performed immediately after drying to evaluate the catalytic behaviour of the as-prepared samples for CO oxidation. Figure 1a shows the corresponding light-off curves (1st run). CO conversion at 25°C is in the range 8–76%. Lowering the temperature and pressure of oxygen during drying has a detrimental effect on the activity (compare light-off curves of H-A-120 with H-A-30, and H-A-30 with H-V-30 and H-H-30, respectively). The most active catalyst is the one dried in air at 120°C. Figure 1b shows the light-off curves for the 2nd run using the same samples. CO conversion improves and is in the range 20–96% (see also Table 1). Thus, exposing the catalysts to high temperature (400°C for 0.5 h) under reaction conditions improves their activity. The CO conversion over the H-H-30 catalyst is low during both the 1st and the 2nd run.

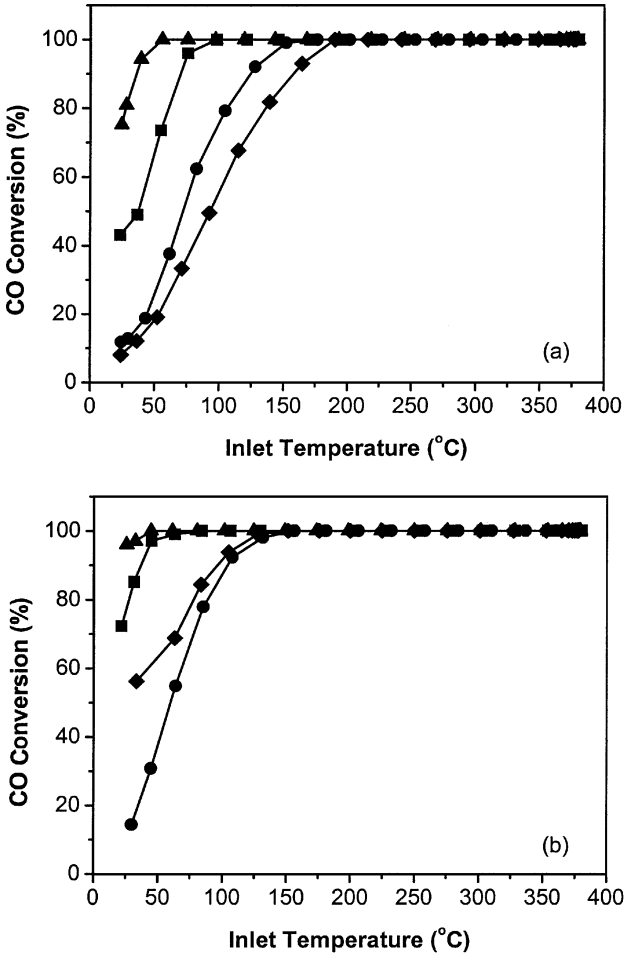

FIG. 1. Light-off curves of Au–Mn co-precipitates of H-A-30 (■), H-A-120 (▲), H-V-30 (◆) and H-H-30 (●) for CO oxidation: (a) 1st run; (b) 2nd run.

Catalyst Characterisation

X-ray diffraction (XRD). The XRD patterns of the catalysts before and after the 1st light-off test are shown in Figs. 2a and 2b, respectively. After drying, the support is mainly manganese carbonate ($MnCO_3$) with small amounts of Mn_3O_4, γ-Mn_2O_3, and possibly MnO. The peak at $2\theta = 13.95^\circ$ is attributed primarily to $MnCO_3$. It is evident that the smallest concentration of $MnCO_3$ exists at H-A-120. Since the XRD pattern of the various Mn compounds have overlapping peaks, it is difficult to distinguish among them. However, comparing Fig. 2a with Fig. 2b, $MnCO_3$ peaks decrease significantly (see for example peaks at $2\theta = 10.83^\circ$ and 13.95°). The above observations are consistent with $MnCO_3$ decomposition to give manganese oxides.

The existence of metallic gold was detected in all samples. The broadening of the diffraction line corresponding to the (422) crystalline phase ($2\theta = 49.12^\circ$) was used to calculate the particle size because all other Au peaks were difficult to deconvolute. In particular, the $2\theta = 16.90^\circ$ peak (Au(111) diffraction line) is positioned very close to the (004) Mn_3O_4 peak at $2\theta = 16.86^\circ$. The average size of the Au particles is displayed in Table 2. The gold particle size is insensitive to the drying procedure, but exposure to high temperature during the light-off test in general increases particle size, possibly due to sintering.

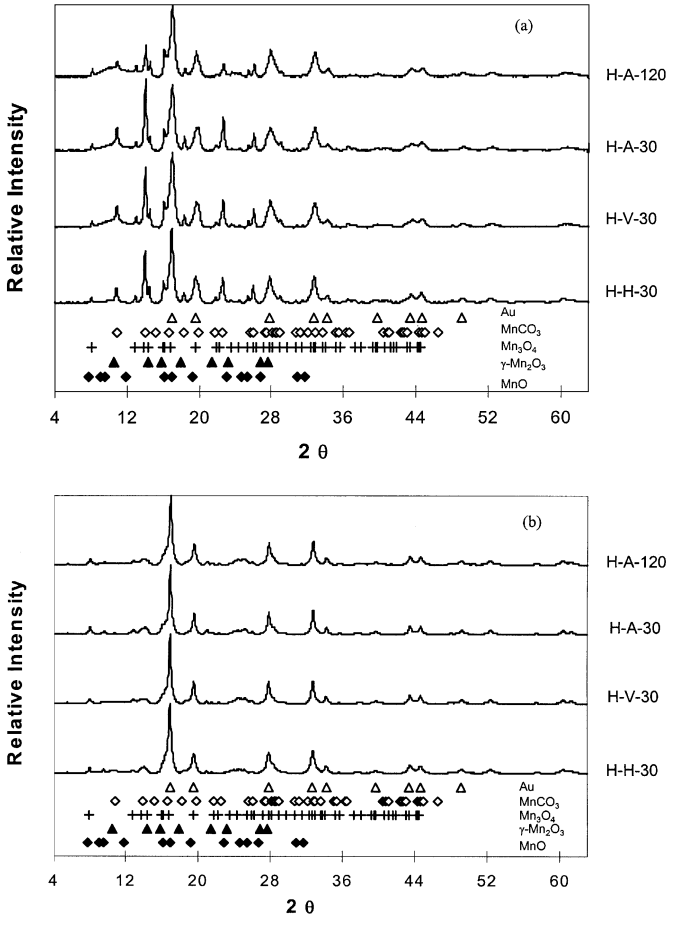

FIG. 2. X-ray diffraction patterns of Au–Mn co-precipitates (a) before first light-off test and (b) after second light-off test.

TABLE 2

Mean Diameter of Au Particles (nm) of Au–Mn Co-precipitates Measured by XRD and TEM

	Before first light-off test		After second light-off test	
	XRD	TEM[a]	XRD	TEM[a]
H-A-120	4.9	4.6 (1.1)	7.5	5.0 (1.3)
H-A-30	4.8	5.0 (1.1)	9.5	5.8 (1.8)
H-V-30	4.7	6.4 (3.0)	9.7	n.d.[b]
H-H-30	6.4	5.5 (1.6)	6.1	5.3 (1.3)

[a] Standard deviation is shown in parentheses.
[b] Not detectable.

Transmission electron microscopy (TEM). Figures 3a and 3b are representative pictures of the H-A-30 catalyst before and after the light-off test. The support has a plate-like shape and the Au particles are mostly rectangular with rounded corners. The manganese support contains an amorphous phase prior to the light-off test. It is quite possible that the amorphous material was formed from the decomposition of $MnCO_3$ by the electron beam during the TEM imaging. *In situ* EDXS and electron diffraction analyses confirmed the elemental composition and crystallinity of the Au nanoparticles that decorated the surface of manganese support. From this figure as well as other TEM pictures (not shown), it is observed that Au particles tend to concentrate on particular regions and this may be due to limitations of the co-precipitation process.

Figure 4 displays the particle size distribution for the catalysts as measured from the TEM micrographs. The distributions are fairly narrow, ranging from 2 to 10 nm. The mean sizes of Au particles in the fresh catalysts are between 4.5 and 6.5 nm and the used ones are always larger than 5.3 nm. As seen in Table 2, particle sizes measured by TEM and XRD are similar, for the fresh catalysts. After the light-off test, the particle size measured by XRD is larger than the one measured by TEM.

^{197}Au Mössbauer spectroscopy. A typical ^{197}Au Mössbauer spectrum of Au–Mn co-precipitates is shown in Fig. 5a. It consists of a single line very similar to that of bulk metallic gold for which an isomer shift of -1.23 mm/s has been observed (29). It is worth noting that spectra of gold oxides and gold chlorides are composed of doublets. Isomer shifts observed for selected samples are summarised in Table 3. The Mössbauer spectra show that gold is always present in metallic form. It is surprising, however, that there is a tendency of the isomer shift to be slightly more negative than that of bulk gold.

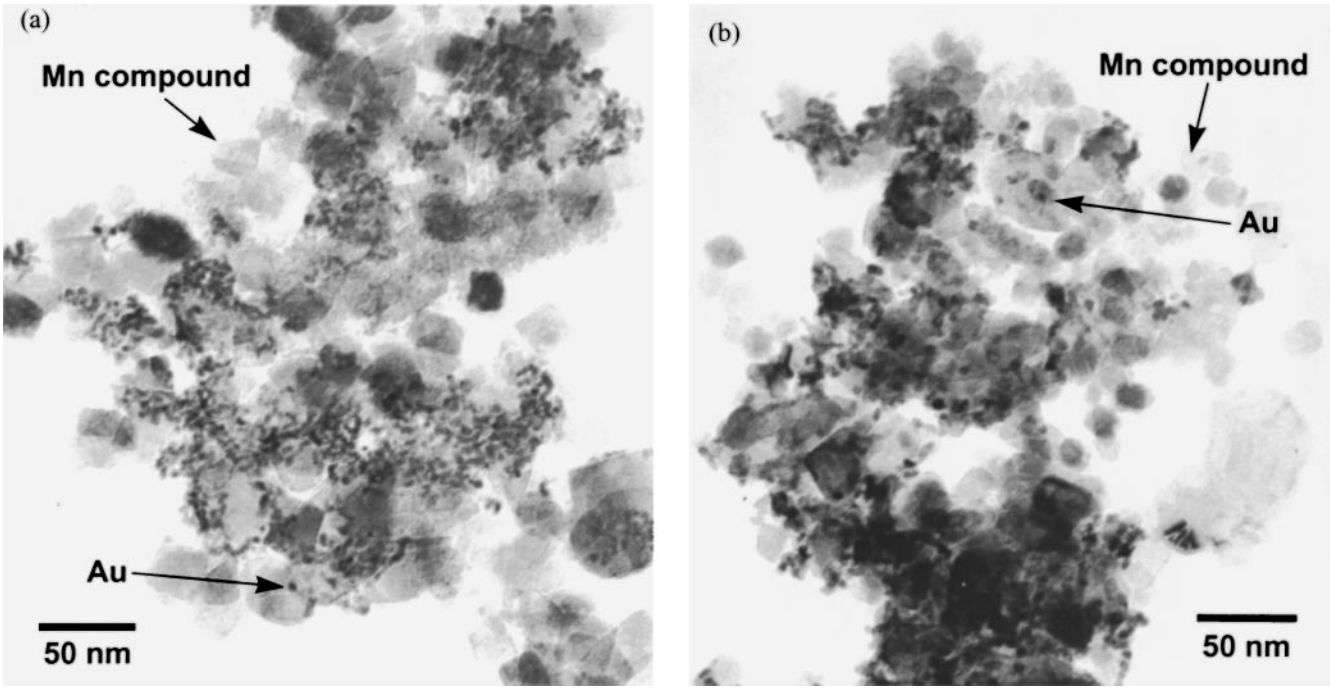

FIG. 3. TEM photographs of H-A-30 (a) before first light-off test and (b) after second light-off test.

Since the starting gold species is Au^{3+}, detection of Au^0 indicates that Au is reduced at some point during the preparation process. To find out when this reduction took place, Mössbauer spectra were obtained immediately after co-precipitation, having quenched the Au–Mn co-precipitate in liquid nitrogen. Figure 5b shows the corresponding ^{197}Au Mössbauer spectrum. Metallic gold appears again and the isomer shift is -1.24 ± 0.01 mm/s, which is similar to those of samples before the light-off test. Accordingly, this indicates that the metallic gold in Au–Mn co-precipitates is produced during the co-precipitation process itself.

X-ray photoelectron spectroscopy (XPS). The XPS survey spectra acquired from the samples before and after the light-off test reveal that the surface of the samples contains gold, manganese, oxygen, carbon, and sodium elements (see Fig. 6). The sodium most likely originates from the sodium carbonate used during catalyst preparation and is trapped in defect locations of Mn-containing crystallites. The absence of chlorine is a good indication of the effectiveness of the washing procedure. Similar observations regarding the presence of sodium and chlorine have also been made by Srinivasan and Gardner (5). A summary of the catalyst's surface composition before and after the light-off test is displayed in Table 4. Before the light-off test, the surface Au/Mn ratios for H-A-120, H-A-30, and H-V-30 are 0.15, 0.16, and 0.18, respectively. These values decrease to 0.10, 0.10, and 0.09, respectively, after the first light-off test (1st run). These results are in agreement with the XRD and TEM data that indicated sintering of Au particles for these catalyst samples *after the reaction*. The H-H-30

TABLE 3

^{197}Au Mössbauer Isomer Shifts of Au–Mn Co-precipitates before and after Light-off Tests

Sample	Isomer shift (mm/s)[a]
H-A-120 before 1st run	−1.23
H-A-30 after 1st run	−1.25
H-H-30 before 1st run	−1.25
H-H-30 after 1st run	−1.27

[a] Experimental error is ca. ±0.01 mm/s.

TABLE 4

Surface Composition (%) of Au–Mn Co-precipitates Analysed by XPS

	Mn *2p*	Au 4*f*	C 1*s*	O 1*s*	Na 1*s*
		Before light-off test			
H-A-120	26.1	3.9	22.6	46.6	0.8
H-A-30	24.9	3.9	23.6	46.8	0.8
H-V-30	25.8	4.7	23.3	45.4	0.8
H-H-30	26.1	3.4	23.3	46.4	0.8
		After light-off test			
H-A-120	32.8	3.2	19.2	43.3	1.5
H-A-30	32.8	3.3	18.7	43.7	1.5
H-V-30	31.3	2.7	19.5	45.3	1.2
H-H-30	29.9	3.7	21.6	44.0	0.8

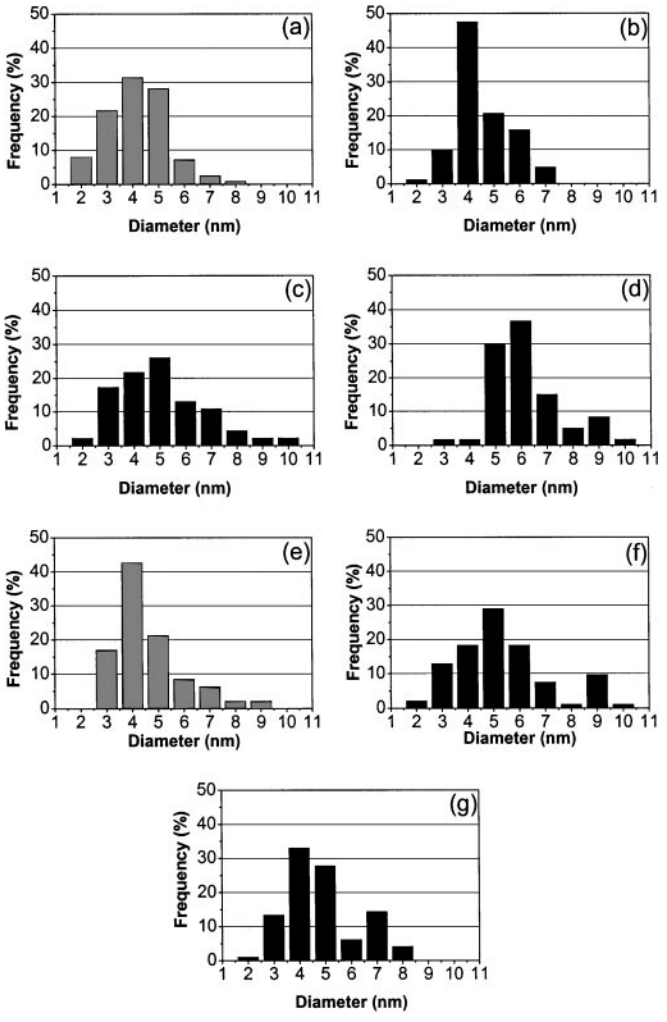

FIG. 4. Size distribution of Au–Mn co-precipitates: (a) H-A-120 before light-off test, (b) H-A-30 before light-off test, (c) H-H-30 before light-off test, (d) H-V-30 before light-off test, (e) H-A-120 after light-off test, (f) H-A-30 after light-off test, and (g) H-H-30 after light-off test.

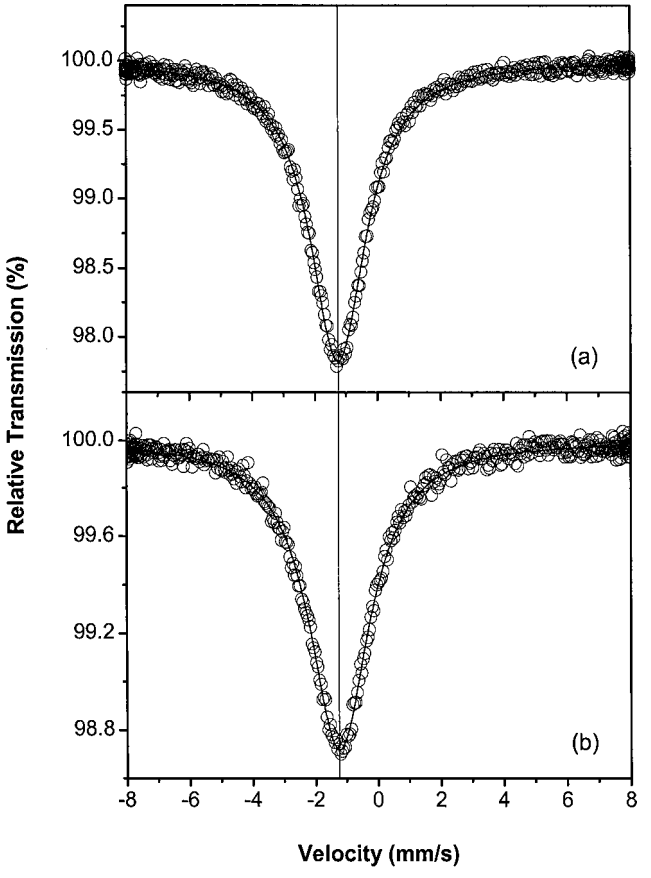

FIG. 5. ^{197}Au Mössbauer spectra for (a) sample dried in air at 120°C (H-A-120 before light-off test) and (b) sample quenched in liquid nitrogen immediately after co-precipitation of Au and Mn compounds.

catalyst, which has the same particle size before and after the light-off test (cf. Table 2), also has the same surface Au/Mn ratios before and after the light-off experiment.

The high-resolution XPS spectra of Au 4*f*, Mn 2*p*, C 1*s*, and O 1*s* are shown in Figs. 7 and 8 for catalyst samples before and after the light-off test. An examination of the XPS spectra for Au 4*f* (84 eV) indicates that the Au nanoparticles are metallic even before the light-off test (see Fig. 7a). This is in agreement with the results of ^{197}Au Mössbauer spectroscopy. After the light-off test (see Fig. 8a), the binding energy of the Au 4*f* is slightly larger than that of bulk Au (84.1 eV) but considerably smaller than that of Au_2O_3 (~86 eV), AuCl (~85.9 eV), $HAuCl_4$ (~87.4 eV), and $Au(OH)_3$ (87.7 eV)(34). The Au 4*f* binding energies of H-A-120 and H-A-30 increase by 0.2–0.4 eV while in H-H-30 and H-V-30 the shift of the binding energy is not significant.

Figures 7b and 8b display the Mn 2*p* XPS spectra acquired from the samples before and after the light-off test, respectively. Figure 7b shows the Mn $2p_{3/2}$ peak located at 642.3 eV along with two weak satellite peaks at 647 and 665 eV. These indicate the presence of $MnCO_3$, MnO_2, MnO, Mn_3O_4, and Mn_2O_3 (35–37). A smaller satellite feature near 647 eV after the light-off test suggests that a

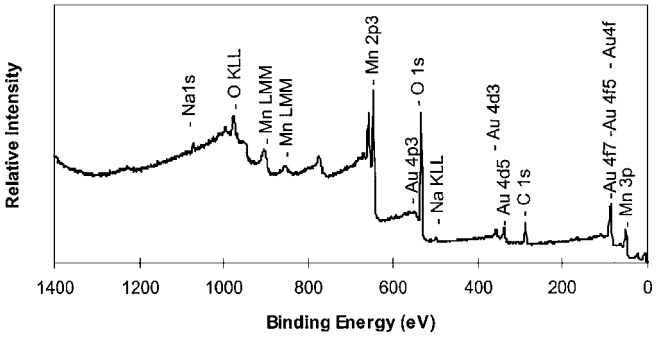

FIG. 6. A typical survey XPS spectrum of Au–Mn co-precipitates (H-A-120).

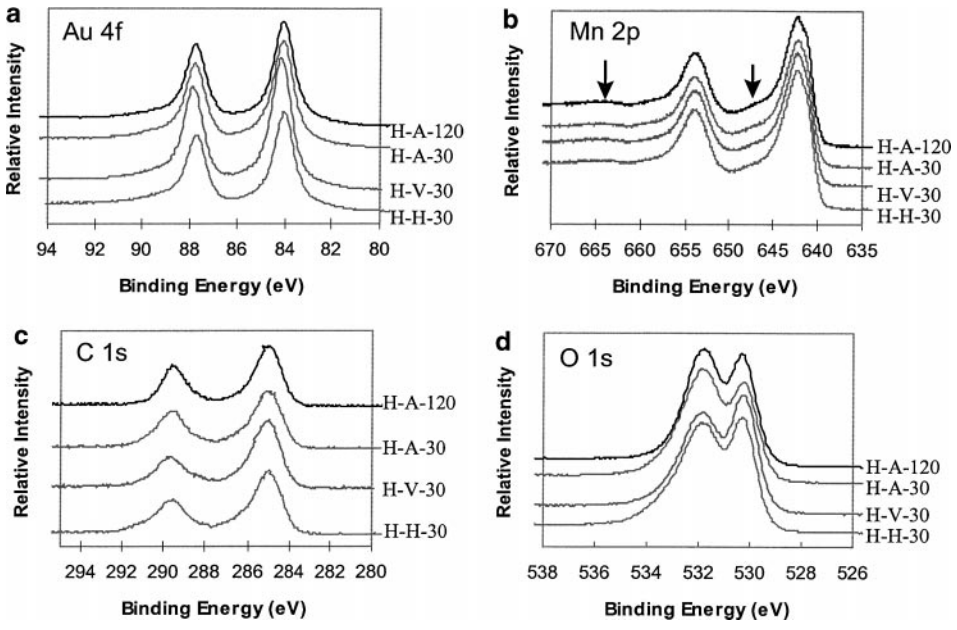

FIG. 7. XPS spectra of (a) Au 4*f*, (b) Mn 2*p*, (c) C 1*s*, and (d) O 1*s* of Au–Mn co-precipitates before light-off test dried in air at 120°C (H-A-120), in air at 30°C (H-A-30), in vacuum at 30°C (H-V-30), and in hydrogen at 30°C (H-H-30).

decrease in the Mn^{2+} species (most likely $MnCO_3$) had occurred (cf. Fig. 9). It is important to note that a shoulder (cf. Figs. 8b and 9) is observed at 639.2 eV of metallic Mn binding energy (35) in the samples after the reaction. However, it is not possible to quantify the relative amount of the metallic Mn in each sample since the shoulder corresponding to metallic Mn is too weak.

The presence of manganese carbonate is also evident from the C 1*s* and O 1*s* spectra shown in Figs. 7c and 7d. In Fig. 7c, the peak at ~285 eV arises from adsorbed contaminants originating from atmospheric CO, CO_2, and hydrocarbons, while the peak at ~289 eV is attributed to metal carbonates (37). The O 1*s* peak near 531.8 eV is usually assigned to carbonate (~531.5 eV), transition metal

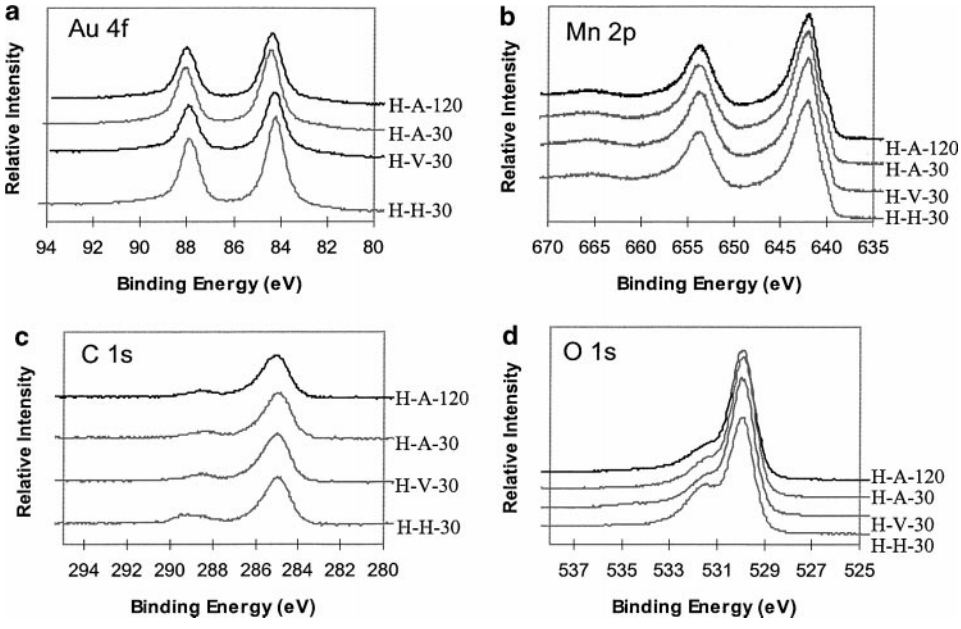

FIG. 8. XPS spectra of (a) Au 4*f*, (b) Mn 2*p*, (c) C 1*s*, and (d) O 1*s* of Au–Mn co-precipitates after light-off test dried in air at 120°C (H-A-120), in air at 30°C (H-A-30), in vacuum at 30°C (H-V-30), and in hydrogen at 30°C (H-H-30).

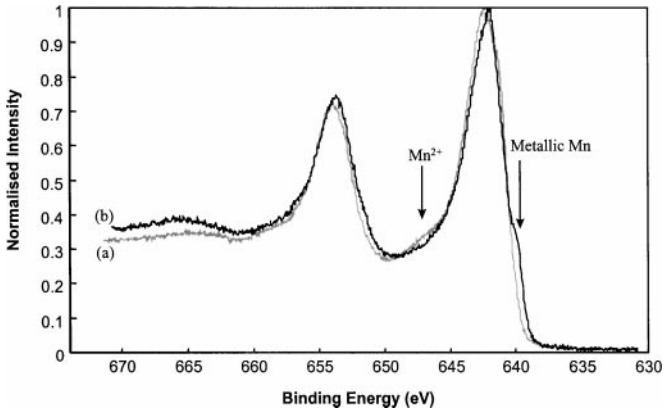

FIG. 9. Mn 2*p* XPS spectra of H-A-120 (a) before light-off test and (b) after light-off test.

hydroxides (∼531.5 eV), and hydroxyl (∼532 eV) (5, 37). The O 1*s* peak at ∼530 eV is close to the binding energies reported by Shirinivasan and Gardner (5) for MnO (529.6 eV and 530.8 eV), Mn_3O_4 (529.6 eV), Mn_2O_3 (530.1 eV), and MnO_2 (529.7 eV). Following the light-off test, the C 1*s* (∼289.5 eV) and O 1*s* (∼531.5 eV) peaks, corresponding to $MnCO_3$, decrease (compare Figs. 7c and 7d with Figs. 8c and 8d). This is consistent with the disappearance of the carbonate phase as shown in XRD results. The O 1*s* spectrum of H-H-30 (Fig. 7d) shows a small shoulder at 533.5 eV, which is caused by the hydrogenation of the carbonate group.

DISCUSSION

Physical and Chemical Properties of the Supported Gold Particles

The gold particles before the light-off test are 4.5–6.5 nm in size as measured by XRD and TEM, and their surface morphology can be described as a rectangle with rounded corners. The XPS and ^{197}Au Mössbauer spectroscopy of freshly dried Au–Mn co-precipitates indicate that the Au is metallic even before the light-off test. Furthermore, ^{197}Au Mössbauer of the sample quenched immediately after co-precipitation reveals only metallic gold. This suggests that Au metal is formed during co-precipitation rather than during the drying stage. It is worth noting that when gold is precipitated with iron compounds under similar preparation conditions, both metallic gold and oxidic species such as gold oxide and oxyhydroxide were observed in dried gold/iron oxide catalysts (29, 38, 39). If low-valence iron species are present in solution (Fe^{2+}), a redox reaction between Fe^{2+} and $AuCl_4^-$ can take place, specially at high pH, which results in the formation of metallic gold (38). It is possible that something similar happens in our system since we start from low-valence manganese (Mn^{2+}). Thermodynamically favoured redox reactions between Mn^{2+} and Au species, taking place at high pH, can result in the formation of Au^0 and high-valence manganese oxides, as observed experimentally.

The Au particle sizes are slightly different between the samples before the light-off test. Miyamoto *et al.* (40) demonstrated using molecular dynamics that Au atoms in their cluster have mobility and the clusters can be aggregated on the MgO(100) plane even at a temperature of 300 K. Also, it was experimentally observed that coalescence behaviour of small gold particles is influenced by particle size and substrate on which the particles are deposited (41). In this study, very small Au particles aggregated on Mn compounds, which was probably dependent on the surface of the Mn compounds.

The gold nanoparticles in general show significantly smaller isomer shifts than bulk gold (Table 2). This is in good agreement with a similar observation for gold particles of various sizes embedded in a Mylar matrix (42), where it was found that the isomer shifts of the metallic gold cores of the nanoparticles ranged from −1.23 mm/s for particles of diameter 10 nm or more to −1.30 mm/s for particles of diameter 3 nm. This shift to more negative velocities reflects a lower *s*-electron density at the nuclei compared to that of bulk Au metal. One reason for this could be lattice expansion in the nanoscale Au particles, but this does not appear to be the case here, as the Au lattice constants calculated from the Au(422) lines in the XRD data were in the range 4.074–4.078 Å, which is slightly smaller than the 4.079 Å of bulk Au metal. A similar small lattice contraction with decreasing size was also reported in the Au on Mylar nanoparticles (42). The most likely explanation for the lowered *s*-electron density is that there is a net electron flow toward the particle surface, which more than compensates for the increase of the *s*-electron density induced by the lattice contraction (42). Such electron transfer effects have also been reported in studies of Au_{55} clusters and are attributed in part to ligand bonding at the cluster surface (43). We conclude that our samples show evidence of electron transfer effects of a type that would be expected for gold nanoparticles in close contact with the support matrix.

Since after the second light-off test larger gold particles are detected, sintering must have taken place after exposure to high temperatures. Although the Au crystallites measured by XRD are not necessarily the same as the Au particles detected by TEM, the discrepancy between particle sizes measured by XRD and TEM after the light-off test seems to be larger as compared with sizes of the fresh catalysts. A reason for that may be limitations of the measurement techniques. Namely, a well-defined X-ray diffraction pattern can be obtained only for crystallites larger than 50 Å(44). Therefore, a small number of relatively large particles could bias the XRD measurement but be difficult to spot in the TEM.

The chemical state of gold particles after the light-off test is similar to metallic gold. However, after the light-off test the Au 4*f* binding energy shifts toward higher values by 0.2–0.4 eV from the 84.1 eV corresponding to bulk metallic gold. Similar higher binding energies have been observed in several supported gold catalyst systems such as Au/Fe_2O_3 (14, 32), Au/Co_3O_4 (32), and Au/MnO_x (5) catalysts. The shift of binding energy has been attributed to various phenomena including, "chemical shift" due to chemical bonding or electron transfer or "matrix effects" associated with differences in crystal potential, work function, and relaxation energy (cf. 45, 46).

Matrix effects become important for small particles, where Au loses its metallic character. Kim and Winograd (45) observed a Au 4*f* binding energy shift when the gold layer thickness deposited on SiO_2 was below 1 Å. Furthermore, Au particles supported on graphite were reported to lose their metallic character when their size was smaller than 20 Å (47). Since Au particles in our work are larger than 20 Å, "matrix effects" are not expected to be important. The "chemical shift" can be due to metal–support interaction or a change of the Au oxidation state. The latter is unlikely since oxidic Au would create a much larger binding energy shift (at least 1.8 eV) than the one observed (0.2–0.4 eV). Therefore, the shift of Au 4*f* binding energy in our catalysts after the light-off test is likely due to metal–support interaction such as electron transfer from Au to Mn oxides. It has been reported that Pd/CeO_2 catalysts prepared by deposition–precipitation show a binding energy of Pd 3*d* existing between palladium metal and Pd^{1+} (48). Furthermore, it has been suggested that the slightly oxidic Pd was produced by electron transfer from palladium to ceria, showing the strong interaction between palladium particles and support.

Physical and Chemical Properties of the Mn-Compound Support

The primary phase of the freshly precipitated and dried substrate was found by XRD to be manganese carbonate in all cases, which is consistent with the result obtained by Haruta's group (9). As mentioned earlier, manganese oxides such as MnO, Mn_2O_3, Mn_3O_4, and MnO_2 are also present. The XRD data indicated different $MnCO_3$ concentrations, the lowest being for H-A-120.

The various Au/Mn ratios of samples before the light-off test may be due to a change of Mn concentration rather than that of Au concentration in the samples. It is well known that pure $MnCO_3$ slowly darkens in air through air oxidation and CO_2 begins to evolve below 100°C, leaving MnO (49). Thus, the air oxidation results probably in the increase of Mn concentration on the surface of the samples. Something similar may have occurred in sample H-H-30 by hydrogenation of the carbonate group, as proven with a shoulder in the O 1*s* XPS spectrum of H-H-30 before the light-off test. A higher XPS O 1*s* peak at 531.8 eV attributed to $MnCO_3$ *and* hydroxyl groups is observed for samples H-A-120 and H-A-30. Thus, it is possible that the H-A-120 and H-A-30 contain more hydroxyl groups than the other samples. It is worth noting that hydroxyl groups on MnO_2 can be present even after being heated at 200°C (50). However, it is difficult to confirm the presence of hydroxyl groups only with XPS spectra because an ultra-high vacuum was utilised in the XPS measurements.

The 1st run and the subsequent heat treatment (i.e., 400°C for 0.5 h in the reaction mixture) results in decomposition of $MnCO_3$ as evidenced by XRD and XPS (i.e., Mn 2*p*, C 1*s*, and O 1*s*) results. The process is known to be dependent on temperature and treatment atmosphere. Torres Sanchez *et al.* (9) observed $MnCO_3$ decomposition after reaction (CO and H_2 oxidation) at 120°C and suggested that this decomposition is important for stable activity of the catalyst. Hegedüs and Martin (51) showed that decomposition in nitrogen started at ca. 250°C while in CO_2 at ca. 400°C. However, hydrogenation of carbonate in H-H-30 leads to poorer conversion of the manganese carbonate into MnO_x as indicated by both the XPS (Figs. 8c and 8d) and XRD (Fig. 2) results.

In addition to decomposition of $MnCO_3$, it was observed that metallic Mn is present especially in samples after the light-off test. Such metallic manganese is usually related to strong metal–support interactions (SMSI). It has been suggested that SMSI effects are caused by electron transfer between the support and metal or by intermetallic compounds of support and metal atoms (52). In this study, intermetallic Au_xMn_y alloy was not observed in the ^{197}Au Mössbauer spectrum of H-A-30 after the light-off test. An isomer shift from intermetallic compounds should appear in a positive direction from metallic gold and should be a linear function of the atomic percentage of manganese (53). Thus, the metallic Mn is associated with a SMSI resulting from electron transfer between the support and metal especially from Au metal to MnO_x support as proven by the Au 4*f* XPS spectra.

Catalytic Performance of Au–Mn Co-precipitates

As shown earlier in Table 1, room-temperature catalyst activity depends on the drying conditions employed. The most active catalyst is the one dried in air at 120°C. Furthermore, catalysts dried in air are more active than those dried in vacuum or hydrogen (compare H-A-30 with H-V-30 and H-H-30). With the exception of H-H-30, the catalyst activity correlates well with the surface Au/Mn ratio. The activity increases as the Au/Mn ratio of the catalysts decreases from 0.18 (H-V-30) to 0.15 (H-H-120). The H-H-30 with its partially hydrogenated carbonate surface exhibits the lowest activity even though it has a lower Au/Mn ratio of 0.13. This may be due to the difference in the surface chemistry of H-H-30 catalyst as compared to those dried in

the presence of oxygen. Another reason for the difference in activity between H-A-120 and H-A-30 before the light-off test may be the high concentration of $MnCO_3$ on the latter (see Fig. 2a).

Catalyst performance is improved at the 2nd light-off test, i.e., after it has been exposed to high temperatures during the 1st light-off test (see Table 1 and compare Figs. 1a and 1b). After the light-off test, the surface Au/Mn ratio decreases by a third to half of the original values. The lower Au/Mn ratio is possibly due to the sintering of the Au particles as indicated by XRD and TEM measurements or to the transformation of the manganese carbonate to manganese oxides. The decrease in surface Au/Mn ratio coincides with the enhancement in the catalyst activity for low-temperature CO oxidation. It is interesting to note that the activity is higher for catalysts (H-A-120 and H-A-30) with a Au/Mn ratio close to 0.1. The least active catalyst, H-H-30, retained a significant amount of surface carbonate after the light-off experiment and displayed the same Au/Mn ratio of 0.13 as the starting fresh catalyst.

Grunwaldt *et al.* (27, 28) reported that heating in a gas mixture of CO and O_2 fully activates Au/TiO_2 catalyst, even though dried Au/TiO_2 catalysts are readily active without further calcination. The enhancement of catalytic performance was attributed to support interactions, which lead to an increase in the number of low-coordinated gold sites that are responsible for CO oxidation. Haruta *et al.* (46) and Tsubota *et al.* (17) argue that high temperature induces strong metal–support interactions and electron transfer from the gold metal to the support, which are beneficial for low-temperature CO oxidation. In our system the presence of metal–support interactions is evidenced by the shift of the Au $4f_{7/2}$ binding energy by ca. 0.2 eV and the presence of the metallic Mn. It must be pointed out that all of our Au/MnO_x catalysts are active for low-temperature CO oxidation even without calcination, while Tsubota *et al.* (17, 54) reported that Au/TiO_2 does not display low-temperature catalytic activity unless it is heated to temperatures higher than 200°C.

The order of catalyst activity in the 2nd run may be related to Na surface concentration. From Tables 1 and 4, it can be seen that samples having high Na surface concentration exhibit higher activity. It is worth noting that Hoflund *et al.* (7) observed a dependence of catalytic activity of Au/MnO_x on alkali metal ions including Li^+, Na^+, and K^+. They proposed that the existence of alkali metal ions on the Au/MnO_x catalysts may suppress retention of carbon dioxide. Thus, a similar Na promoting effect may be present in our study.

The activity of the catalysts in this work is comparable to that of Au/MnO_x prepared using similar methods by Gardner *et al.* (3). Higher activities have been reported by Torres Sanchez *et al.* (9) and this may be due to the fact that excess oxygen and lower flow rates were utilised in their experiments.

CONCLUSIONS

Au/MnO_x catalysts were prepared by co-precipitation and they were found to contain only metallic gold, which was produced during the co-precipitation procedure. The support consisted of manganese carbonate and manganese oxides such as MnO, Mn_2O_3, Mn_3O_4, and MnO_2. The samples showed catalytic activity even without a calcination step. Manganese carbonates decomposed after the light-off test. The mean gold particle size ranged from 4.5 to 6.5 nm for the samples before the light-off test, and it increased slightly after the 2nd light-off test. Catalysts dried in air showed higher CO conversion than those dried in vacuum or hydrogen. Subsequent heat treatment at 400°C (i.e., 1st light-off test) enhanced the activity. This enhancement was associated with the shift of Au 4*f* binding energy and the presence of metallic Mn caused by strong interaction between metallic gold and the substrate, the transformation of $MnCO_3$ to MnO_x, and high surface Na concentration.

ACKNOWLEDGMENTS

We thank the British Council and Deutscher Akademischer Austauschdienst for their support of an Academic Research Collaboration that facilitates this work, Dr. K. Moulding of MCPE, HKUST, HK for the TEM analysis, Andrew Steer of the University College London, and Mark Roberts of the CLRC Daresbury Laboratory for their assistance with the synchrotron X-ray diffraction experiments.

REFERENCES

1. Haruta, M., *Catal. Today* **36**(1), 153 (1997).
2. Bond, G. C., and Thompson, D. T., *Catal. Rev.–Sci. Eng.* **41**(3–4), 319 (1999).
3. Gardner, S. D., Hoflund, G. B., Schryer, D. R., Schryer, J., Upchurch, B. T., and Kielin, E. J., *Langmuir* **7**(10), 2135 (1991).
4. Ando, M., Kobayashi, T., and Haruta, M., *J. Chem. Soc. Faraday Trans.* **90**(7), 1011 (1994).
5. Srinivasan, B., and Gardner, S. D., *Surf. Interface Anal.* **26**(13), 1035 (1998).
6. Gardner, S. D., Hoflund, G. B., Upchurch, B. T., Schryer, D. R., Kielin, E. J., and Schryer, J., *J. Catal.* **129**(1), 114 (1991).
7. Hoflund, G. B., Gardner, S. D., Schryer, D. R., Upchurch, B. T., and Kielin, E. J., *Appl. Catal. B* **6**(2), 117 (1995).
8. Hoflund, G. B., Gardner, S. D., Schryer, D. R., Upchurch, B. T., and Kielin, E. J., *Langmuir* **11**(9), 3431 (1995).
9. Torres Sanchez, R. M., Ueda, A., Tanaka, K., and Haruta, M., *J. Catal.* **168**(1), 125 (1997), doi:10.1006/jcat.1997.1636.
10. Bamwenda, G. R., Tsubota, S., Nakamura, T., and Haruta, M., *Catal. Lett.* **44**(1–2), 83 (1997).
11. Hutchings, G. J., Siddiqui, M. R. H., Burrows, A., Kiely, C. J., and Whyman, R., *J. Chem. Soc. Faraday Trans.* **93**(1), 187 (1997).
12. Haruta, M., Kageyama, H., Kamijo, N., Kobayashi, T., and Delannay, F., *in* "Successful Design of Catalysts" (T. Inui, Ed.), p. 33. Elsevier, Amsterdam, 1988.
13. Haruta, M., Yamada, N., Kobayashi, T., and Iijima, S., *J. Catal.* **115**(2), 301 (1989).
14. Haruta, M., Tsubota, S., Kobayashi, T., Kageyama, H., Genet, M. J., and Delmon, B., *J. Catal.* **144**(1), 175 (1993), doi:10.1006/jcat.1993.1322.

15. Haruta, M., Ueda, A., Tsubota, S., and Sanchez, R. M. T., *Catal. Today* **29**(1–4), 443 (1996).
16. Tsubota, S., Haruta, M., Kobayashi, T., Ueda, A., and Nakahara, Y., *in* "Preparation of Catalysts V" (G. Poncelet *et al.*, Eds.), p. 695. Elsevier, Amsterdam, 1991.
17. Tsubota, S., Cunningham, D. A. H., Bando, Y., and Haruta, M., *in* "Preparation of Catalysts VI" (G. Poncelet *et al.*, Eds.), p. 227. Elsevier, Amsterdam, 1995.
18. Tsubota, S., Cunningham, D. A. H., Bando, Y., and Haruta, M., *Catal. Lett.* **31**(2–3), 133 (1995).
19. Iizuka, Y., Tode, T., Takao, T., Yatsu, K., Takeuchi, T., Tsubota, S., and Haruta, M., *J. Catal.* **187**(1), 50 (1999), doi:10.1006/jcat.1999.2604.
20. Okumura, M., Tanaka, K., Ueda, A., and Haruta, M., *Solid State Ionics* **95**(1–2), 143 (1997).
21. Okumura, M., Nakamura, S., Tsubota, S., Nakamura, T., Azuma, M., and Haruta, M., *Catal. Lett.* **51**(1–2), 53 (1998).
22. Yuan, Y. Z., Asakura, K., Wan, H. L., Tsai, K., and Iwasawa, Y., *Catal. Lett.* **42**(1–2), 15 (1996).
23. Yuan, Y. Z., Kozlova, A. P., Asakura, K., Wan, H. L., Tsai, K., and Iwasawa, Y., *J. Catal.* **170**(1), 191 (1997), doi:10.1006/jcat.1997.1752.
24. Kozlova, A. P., Sugiyama, S., Kozlov, A. I., Asakura, K., and Iwasawa, Y., *J. Catal.* **176**(2), 426 (1998), doi:10.1006/jcat.1998.2069.
25. Liu, H. C., Kozlov, A. I., Kozlova, A. P., Shido, T., and Iwasawa, Y., *Phys. Chem. Chem. Phys.* **1**(11), 2851 (1999).
26. Grunwaldt, J. D., and Baiker, A., *J. Phys. Chem. B* **103**(6), 1002 (1999).
27. Grunwaldt, J. D., Kiener, C., Wogerbauer, C., and Baiker, A., *J. Catal.* **181**(2), 223 (1999), doi:10.1006/jcat.1998.2298.
28. Grunwaldt, J. D., Maciejewski, M., Becker, O. S., Fabrizioli, P., and Baiker, A., *J. Catal.* **186**(2), 458 (1999), doi:10.1006/jcat.1999.2564.
29. Wagner, F. E., Galvagno, S., Milone, C., Visco, A. M., Stievano, L., and Calogero, S., *J. Chem. Soc. Faraday Trans.* **93**(18), 3403 (1997).
30. Cunningham, D., Tsubota, S., Kamijo, N., and Haruta, M., *Res. Chem. Interm.* **19**(1), 1 (1993).
31. Tanielyan, S. K., and Augustine, R. L., *Appl. Catal. A* **85**(1), 73 (1992).
32. Epling, W. S., Hoflund, G. B., Weaver, J. F., Tsubota, S., and Haruta, M., *J. Phys. Chem.* **100**(23), 9929 (1996).
33. Gardner, S. D., Hoflund, G. B., Davidson, M. R., Laitinen, H. A., Schryer, D. R., and Upchurch, B. T., *Langmuir* **7**(10), 2140 (1991).
34. Park, E. D., and Lee, J. S., *J. Catal.* **186**(1), 1 (1999), doi: 10.1006/jcat.1999.2531.
35. Di Castro, V., and Polzonetti, G., *J. Electron Spectrosc. Relat. Phenom.* **48**, 117 (1989).
36. Foord, J. S., Jackman, R. B., and Allen, G. C., *Philos. Mag. A* **49**(5), 657 (1984).
37. Zhao, L. Z., and Young, V., *J. Electron Spectrosc. Relat. Phenom.* **34**, 45 (1984).
38. Greffié C., Benedetti, M. F., Parron, C., and Amouric, M., *Geochim. Cosmochim. Acta* **60**(9), 1531 (1996).
39. Finch, R. M., Hodge, N. A., Hutchings, G. J., Meagher, A., Pankhurst, Q. A., Siddiqui, M. R. H., Wagner, F. E., and Whyman, R., *Phys. Chem. Chem. Phys.* **1**(3), 485 (1999).
40. Miyamoto, A., Hattori, T., Kubo, M., and Inui, T., *in* "Computer Aided Innovation of New Materials II" (M. Doyama *et al.*, Eds.), p. 1021. Elsevier, Amsterdam, 1993.
41. Iijima, S., and Ajayan, P. M., *J. Appl. Phys.* **70**(9), 5138 (1991).
42. Stievano, L., Santucci, S., Lozzi, L., Calogero, S., and Wagner, F. E., *J. Non-Cryst. Solids* **234**, 644 (1998).
43. Mulder, F. M., v.d. Zeeuw, E. A., and Thiel, R. C., *Solid State Commun.* **85**(2), 93 (1993).
44. Heck, R. M., and Farrauto, R. J., "Catalytic Air Pollution Control: Commercial Technology." Van Nostrand Reinhold, New York, 1995.
45. Kim, K. S., and Winograd, N., *Chem. Phys. Lett.* **30**(1), 91 (1975).
46. Haruta, M., Kobayashi, T., Iijima, S., and Delannay, F., *in* "Proceedings, 9th International Congress on Catalysis, Calgary 1988" (M. J. Phillips and M. Ternan, Eds.), Vol. 3, p. 1206. Chem. Institute of Canada, Ottawa, 1988.
47. Rao, C. N. R., Santra, A. K., and Vijayakrishnan, V., *Top. Catal.* **1**, 25 (1994).
48. Shen, W. J., Ichihashi, Y., Okumura, M., and Matsumura Y., *Catal. Lett.* **64**(1), 23 (2000).
49. Sidgwick, N. V., "The Chemical Elements And Their Compounds: Volume II." Oxford Univ. Press, London, 1950.
50. Lee, J. A., Newnham, C. E., Stone, F. S., and Tye, F. L., *J. Colloid Interface Sci.* **45**, 289 (1973).
51. Hegedüs, A. J., and Martin, K., *Mikrochim. Acta* **4–5**, 833 (1966).
52. Foger, K., *in* "Catalysis—Science and Technology" (J. R. Anderson and M. Boudart, Eds.), Vol. 6, p. 288. Springer-Verlag, Berlin, 1984.
53. Parish, R. V., *in* "Mössbauer Spectroscopy Applied to Inorganic Chemistry" (G. J. Long, Ed.), Vol. 1, p. 606. Plenum, New York, 1984.
54. Tsubota, S., Nakamura, T., Tanaka, K., and Haruta, M., *Catal. Lett.* **56**, 131 (1998).